4 Result

4.1 Cloning and purification of NIBP and Ehoc-1

Since the attempts to produce full-length NIBP and Ehoc-1 in *E. coli* or insect cells remained unsuccessful (data not shown), new experiments were planned to produce fragments of the two proteins, and do functional and structural research on these fragments.

4.1.1 Fragments designing

According to a phylogenetic analysis of the TRAPP II – specific subunits [107], human TRAPP subunits NIBP and Ehoc-1 are not as highly conserved among eukaryotes as the smaller subunits of the TRAPP I complex. However, by multiple sequence alignment analysis, conserved AAs as well as several conserved segments were found along their sequence (see Fig 4.1.1). Presumably, these conserved segments should be involved in specific functions, therefore were retained in all eukaryotes. Since the aim of this work was to study the function and characteristics of the two TRAPP subunits, these conserved segments were considered with special importance in the following studies.

(a) NIBP (1246 AA)

(b) Ehoc-1 (1259 AA)

Fig 4.1.1 Conserved segments in the human proteins NIBP and Ehoc-1, drawn according to [107].

Since very little was known about the internal structure and domain organization of the two proteins, fragments of different size and coverage were designed according to the sequence conservation (Fig 4.1.1), secondary structure prediction with Predict-Protein [108] and disorder prediction with PONDR [109].

Altogether, 14 different fragments were designed for NIBP, while 13 fragments were designed for Ehoc-1 (data not shown). With properly designed primers, these

fragments were amplified from cDNA template (from RZPD) and cloned into the pQLink-H or pGex 6p-1 vectors using restriction endonucleases dependent cloning. The sequence-verified recombinant plasmids were transformed into *E. coli* BL21 (DE3) cells. If soluble expression for any fragment was observed in test expression, the fragment would be expressed in larger scale, and applied to further purification and stability test. In general, the solubility and stability of NIBP and Ehoc-1 fragments were very poor, when they were recombinantly expressed in *E. coli*. Although several fragments could be produced as GST-fusion proteins, they degraded instantly after removal of the GST-tag.

4.1.2 Purification of Ehoc-1 fragment

Finally, only one fragment, Ehoc-1 16-211 (referred as E211), which lies near the N-terminus of Ehoc-1 and covers a large half of the first conserved segment (see Fig 4.1.1 b), could be expressed and purified. First expressed as GST-fusion protein, E211 became less stable after removal of the GST-tag, but could be stabilized in buffer with high salt concentration and glycerol (for instance Ehoc-1 protein buffer, see 2.4).

E211 was purified according to the protocols in 3.2.5 – 3.2.9. Samples were collected during the purification steps and analyzed by SDS-PAGE, as shown in Fig 4.1.2.

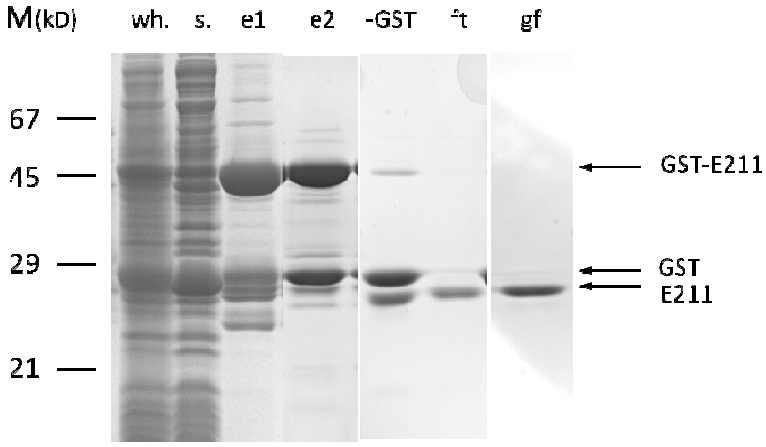

Fig 4.1.2 SDS-PAGE of samples from E211 purification.
wh: whole cell extract; s: supernatant; e1: elution from first affinity chromatography; e2: elution from cation exchange column; -GST: sample after incubation with protease; ft: unbound fractions from the second affinity chromatography column, to remove the GST-tag; gf: peak fractions of gel filtration.

4.2 Structural and biophysical study of NIBP and Ehoc-1

4.2.1 CD spectrum of E211

A CD spectrum between 190 to 260 nm was measured on purified E211, according to the protocol in 3.2.13 (see Fig 4.2.1 a). If compared with the characteristic spectra for different secondary structures (Fig 4.2.1 b), the CD spectrum of E211 suggested that this Ehoc-1 fragment had a distinct structure which is mainly composed of α-helix.

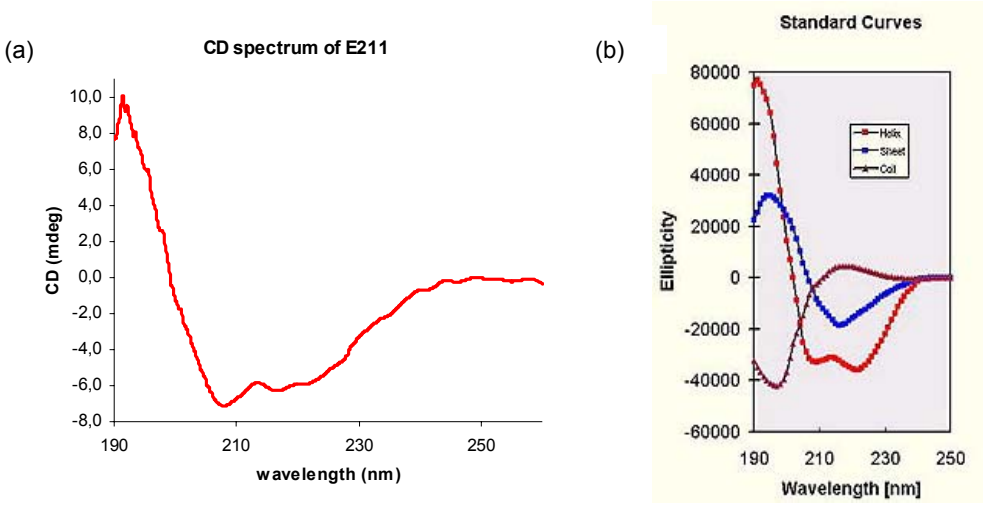

Fig 4.2.1 CD spectrum of E211 suggested a structure mainly composed of α-helix.
(a) CD spectrum of E211, measured between 190 and 260 nm;
(b) Standard CD spectra curves of different secondary structures. Red, α-helix; blue, β-sheet; black, random coil.

4.2.2 Crystallization of E211

Crystallization of E211 was carried out on purified E211 in Ehoc-1 protein buffer at a concentration of 5.7 or 12.5 mg/ml. Initial screens were carried out on 96-well sitting-drop crystallization plates with the commercial crystallization screens pH clear, pH clear II, ComPas, Classic II and JCSG from Qiagen. However, no initial hit was observed so far on any of the crystallization plates.

4.2.3 Interactions of NIBP and Ehoc-1

The interactions between NIBP and Ehoc-1 were studied with co-immuno-precipitation (CoIP) experiments, according to the protocol in 3.4.4. Pairwise interactions between NIBP and Ehoc-1 fragments were studied, which involved the following constructs: flag-tagged NIBP, which was the splice isoform of NIBP, consisting of the AAs 335-1246, or NIBP C, which consisted of AAs 941-1086 and included the fifth conserved segment of NIBP (see Fig 4.1.1 a); with HA-tagged Ehoc-1 N, which consisted of AAs 1-276 and covered most of the first conserved domain in Ehoc-1 (see Fig 4.1.1 b), or Ehoc-1 M, which consisted of AAs 437-544 and corresponded to the second conserved domain of Ehoc-1 (see Fig 4.1.1 b). The resulting immuno-precipitations on α-HA affinity matrix was eluted with 2 x SDS sample buffer and subjected to SDS-PAGE and Western blotting. Cell lysate samples without α-HA affinity matrix were also loaded on the gel as input controls. The blotted membrane was visualized by α-flag and α-HA antibodies (see Fig 4.2.2).

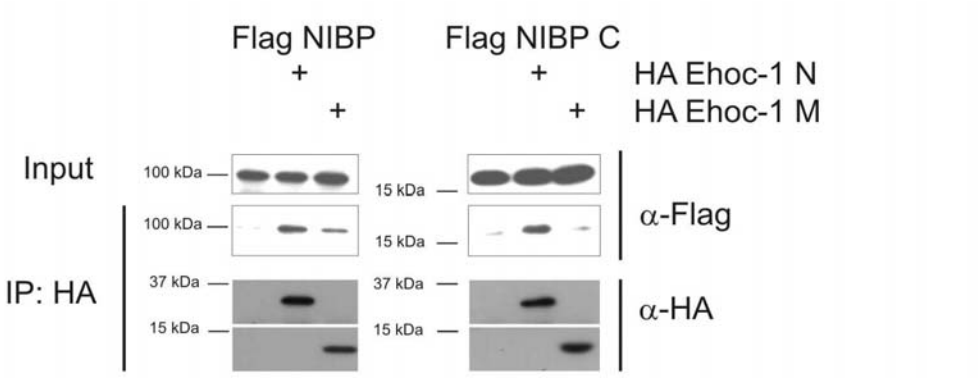

Fig 4.2.2 Co-immuno-precipitation studies with NIBP and Ehoc-1 fragments.
NIBP, NIBP 335-1246; NIBP C, NIBP 941-1086; Ehoc-1 N, Ehoc-1 1-276;
Ehoc-1 M, Ehoc-1 437-544.

From the CoIP results, N-terminally truncated NIBP was shown to bind to an N-terminal fragment (Ehoc-1 N, 1-276), while only weakly to a conserved region from middle part of Ehoc-1 (Ehoc-1 M, 437-544). Furthermore, the interaction with Ehoc-1 fragments was maintained by a shorter fragment of NIBP (NIBP C, 941-1086), from the C-terminal conserved domain of NIBP.

4.3 Structure determination of Tca17

4.3.1 Expression of Tca17 in *E. coli*

The coding region for full-length Tca17 (residues 1-152) was amplified directly from yeast genomic DNA and cloned into the bacterial expression vector pGex-6P1 using *Bam*HI / *Not*I restriction endonucleases. The sequence-verified recombinant plasmid pGex6P1-Tca17 was transformed into *E. coli* BL21(DE3)-T1R cells, and expressed according to the protocol in 3.2.2. Cell pellets from overnight culture were disrupted by Fluidizer treatment.

4.3.2 Purification of Tca17

Tca17 was purified according to the protocols as 3.2.5 – 3.2.9. GST-tagged Tca17 was first purified by a GSH sepharose 4B column, then incubated with PreScission protease at a ratio of 30:1 (Tca17 : protease, w:w), and dialysed against 1 l GST-dialysis buffer at 4 °C overnight. The free GST-tag and uncut GST-Tca17 was removed by a second affinity chromatography step. The unbound fractions from the second affinity column, which mainly contained the tag-free Tca17 protein, were concentrated and loaded on a Superdex 75 gel filtration column equilibrated with Tca17 protein buffer. SeMet labeled Tca17 was purified according to the same protocol, but SeMet Tca17 protein buffer was used instead. Finally the native and SeMet labeled Tca17 protein of higher than 95% purity were produced and concentrated to 12 mg/ml, as required for crystallography experiments. Samples were collected during the purification steps and analyzed by SDS-PAGE, as shown in Fig 4.3.1.

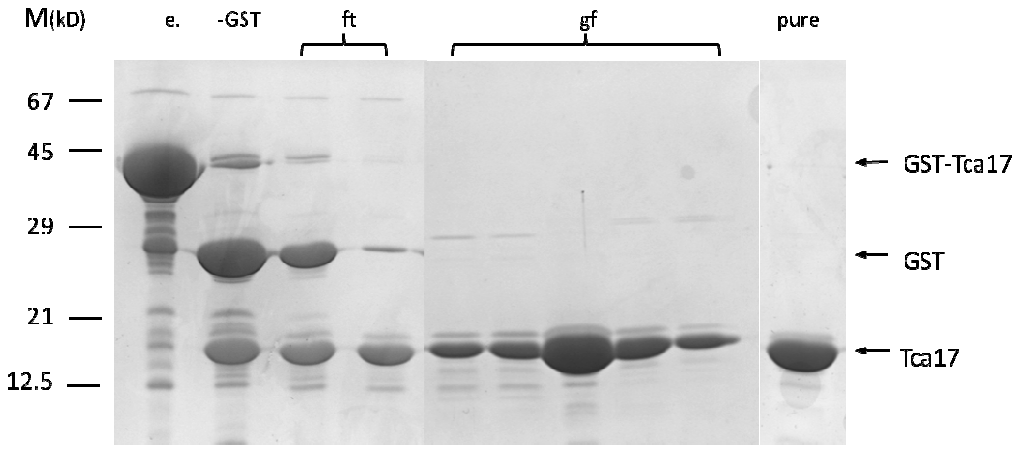

Fig 4.3.1 SDS-PAGE of samples from Tca17 purification.
e: elution from first affinity chromatography;
-GST: sample after incubation with protease;
ft: unbound fractions from two continuous affinity chromatography columns, after the GST-tag was removed by protease digestion;
gf: peak fractions of gel filtration;
pure: purified and concentrated Tca17.

4.3.3 Protein buffer screen

A buffer screen was performed with a fluorescence-based thermal shift assay (protocol as in 3.2.14), to find a suitable stabilizing protein buffer for Tca17.

No.	Buffer condition	T_m1	T_m2	T_m	T_m-T_{mr}
Ref.	20 mM HEPES, pH 8.0,150 mM NaCl	54.60	51.30	52.95	0.00
1	20 mM Na-Ac, pH 5.0, 150 mM NaCl	41.80	41.80	41.80	-11.15
2	20 mM Na-Ac, pH 5.0, 150 mM NaCl, 5% glycerol	45.80	41.00	43.40	-9.55
3	20 mM Na-Ac, pH 5.0, 300 mM NaCl	44.60	42.30	43.45	-9.50
4	20 mM Na-Ac, pH 5.0, 300 mM NaCl, 5% glycerol	45.00	44.80	44.90	-8.05
5	20 mM MES, pH 5.5, 150 mM NaCl	46.60	47.80	47.20	-5.75
6	20 mM MES, pH 5.5, 150 mM NaCl, 5% glycerol	48.60	49.30	48.95	-4.00
7	20 mM MES, pH 5.5, 300 mM NaCl	49.30	50.60	49.95	-3.00
8	20 mM MES, pH 5.5, 300 mM NaCl, 5% glycerol	54.10	47.60	50.85	-2.10
9	20 mM MES, pH 6.0, 150 mM NaCl	53.10	53.40	53.25	0.30
10	20 mM MES, pH 6.0, 150 mM NaCl, 5% glycerol	55.10	56.60	55.85	2.90

11	20 mM MES, pH 6.0, 300 mM NaCl	48.30	51.60	49.95	-3.00
12	20 mM MES, pH 6.0, 300 mM NaCl, 5% glycerol	55.60	55.40	55.50	2.55
13	20 mM MES, pH 6.5, 150 mM NaCl	54.90	52.10	53.50	0.55
14	20 mM MES, pH 6.5, 150 mM NaCl, 5% glycerol	55.10	55.90	55.50	2.55
15	20 mM MES, pH 6.5, 300 mM NaCl	55.10	57.10	56.10	3.15
16	20 mM MES, pH 6.5, 300 mM NaCl, 5% glycerol	59.90	60.90	60.40	7.45
17	20 mM HEPES, pH 7.0, 150 mM NaCl	54.60	55.10	54.85	1.90
18	20 mM HEPES, pH 7.0, 150 mM NaCl, 5% glycerol	58.10	/	58.10	5.15
19	20 mM HEPES, pH 7.0, 300 mM NaCl	58.10	52.90	55.50	2.55
20	20 mM HEPES, pH 7.0, 300 mM NaCl, 5% glycerol	60.60	61.40	61.00	8.05
21	20 mM HEPES, pH 7.5, 150 mM NaCl	53.10	53.40	53.25	0.30
22	20 mM HEPES, pH 7.5, 150 mM NaCl, 5% glycerol	55.10	56.20	55.65	2.70
23	20 mM HEPES, pH 7.5, 300 mM NaCl	58.90	56.10	57.50	4.55
24	20 mM HEPES, pH 7.5, 300 mM NaCl, 5% glycerol	57.10	60.60	58.85	5.90
25	Reference buffer				
26	20 mM HEPES, pH 8.0, 150 mM NaCl, 5% glycerol	/	/	/	/
27	20 mM HEPES, pH 8.0, 300 mM NaCl	/	50.60	50.60	-2.35
28	20 mM HEPES, pH 8.0, 300 mM NaCl, 5% glycerol	55.90	58.60	57.25	4.30
29	20 mM Tris-HCl, pH 8.5, 150 mM NaCl	51.30	51.10	51.20	-1.75
30	20 mM Tris-HCl, pH 8.5, 150 mM NaCl, 5% glycerol	54.60	54.60	54.60	1.65
31	20 mM Tris-HCl, pH 8.5, 300 mM NaCl	49.60	61.60	55.60	2.65
32	20 mM Tris-HCl, pH 8.5, 300 mM NaCl, 5% glycerol	55.90	55.90	55.90	2.95

Table 4.3.1 Results of TSA-based buffer screen

Altogether 32 buffer conditions were tested to screen the influences of pH value and the concentration of NaCl and glycerol on the thermostability of Tca17. A commonly used protein buffer condition (20 mM HEPES, pH 8.0, 150 mM NaCl) was used as reference buffer. For each buffer, two measurements were performed yielding the melting temperatures T_m1 and T_m2. An average T_m value was calculated from the results of two measurements and compared with the melting temperature in reference buffer, T_{mr} (results shown in Table 4.3.1 and Fig 4.3.2).

From the results of the thermal shift assay, it was found that: 1) higher salt concentration and addition of 5% glycerol often led to higher melting temperature, as expected; 2) a pH range between 6.5 and 7.5 was preferred. From the two most stabilizing buffers (No. 16 and 20), where the T_m values were significantly higher than in the reference buffer, Tca17 protein buffer was formulated as 20 mM HEPES, pH 7, 300 mM NaCl, 5% glycerol, 2 mM DTT, which was later used as protein buffer in crystallization.

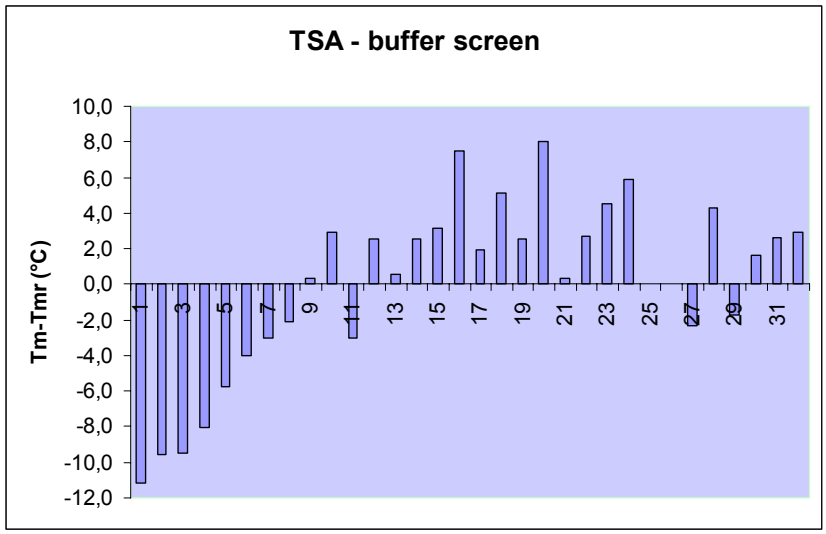

Fig 4.3.2 Melting temperature differences in TSA-based buffer screen

4.3.4 Crystallization of Tca17

Purified Tca17 in Tca17 protein buffer was concentrated to 12 mg/ml and used in crystallization trials. Automated dispensing was performed using the Hydra II pipetting system on 96-well sitting-drop crystallization plates. Reservoir volumes were 75 µl, and the sitting drops were formed by mixing 300 nl protein solution with 300 nl precipitant solution from the same well. Initial screening was carried out with three 96-buffer crystallization screens: JBScreen Basic 1-4, Classics II Suite, and PEGs Suite (see appendix B). Two plates were set up for each screen, and stored separately in 4 °C and 20 °C storage systems. After two weeks, initial crystals were observed on 4 °C plates with precipitant conditions of 20% PEG3350 or PEG4000 and 0.2 M $MgCl_2$. In several rounds of fine screening, the best native and SeMet-labelled Tca17 crystals were obtained from 0.1 M Tris, pH8.5, 0.2 M $MgCl_2$, 20-28% PEG3350, after two months at 4 °C. In order to grow bigger crystals, final fine screens were designed around the best conditions and carried out manually in 24-well hanging-drop plates. Reservoir volumes were 500 µl, and the hanging drops were formed by mixing 1 µl protein with 1 µl precipitant solution.

For data collection, crystals were soaked briefly in cryo-protection solution, and flash frozen in liquid nitrogen. Several different cryo-protection solutions were tested, and the best was composed of reservoir solution with 15% (w/v) PEG 3350 and 15% (v/v) glycerol. Since the SeMet-labeled Tca17 crystals diffracted better than the native crystals, all datasets were collected with SeMet-labeled Tca17 crystals, an image of which in the drop was shown in Fig 4.3.3.

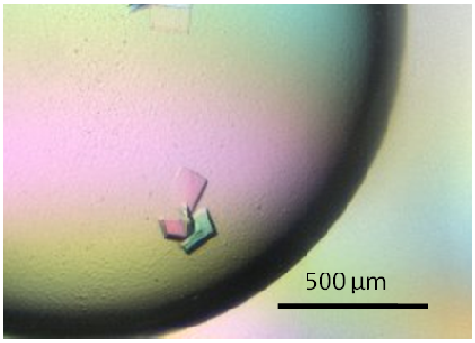

Fig 4.3.3 Crystals of SeMet-labeled Tca17, used to collect MAD datasets.

4.3.5 Data collection and processing

In order to analyze the crystal structure of Tca17, native and MAD datasets were collected at 100 K at beamlines BL 14.1 and BL 14.2 of BESSY, Helmholtz Zentrum Berlin für Materialien und Energie (HZB). For anomalous data collection, an X-ray fluorescence scan was performed on a SeMet Tca17 crystal at the selenium edge and evaluated with the program CHOOCH [110]. The results are listed in Table 4.3.2.

	E (eV)	**λ (Å)**	***f´***	***f´´***
Peak	12,656	0.9796	-7.84	6.22
Inflection	12,654	0.9798	-10.37	3.82
Remote	12,756	0.9720	/	/

Table 4.3.2 Anomalous scattering factors of SeMet Tca17 crystal at three wavelengths

	Anomalous datasets			**Native 1**	**Native 2**
	Peak	**Inflection**	**Remote**		
Wavelength (Å)	0.9797	0.9798	0.9720	0.9919	0.9184
Resolution (Å)	28.96-3.12	29.93-2.99	29.09-3.11	30.01-2.63	29.25-1.80
Outer shell (Å)	3.20-3.12	3.07-2.99	3.19-3.11	2.70-2.63	1.85-1.80
Space group	C2			C2	C2
Unit cell	*a* = 57.24 Å, *b* = 46.75 Å, *c*= 50.48 Å, *β* = 92.92°			*a* = 50.59 Å *b* = 55.45 Å *c*= 57.78 Å *β* = 96.98°	*a* = 57.13 Å *b* = 58.49 Å *c*= 53.97 Å *β* = 92.62°
***I* / *σ*(*I*)**	11.3(2.3)	11.8(1.6)	11.4(1.9)	21.2(2.6)	17.5(3.0)
R_{merge} **(%)**	11.0(74.5)	11.5(93.8)	12.1(76.1)	7.1(73.6)	7.7(58.5)
Unique reflections	4558(323)	5235(396)	4659(342)	4786(358)	16453(1216)
Completeness (%)	98.1(99.1)	98.1(95.4)	97.9(100.3)	99.6(99.4)	99.4(99.5)

Table 4.3.3 Data collection statistics for anomalous and native Tca17 datasets. Values in parentheses refer to the outer shell of reflections.
R_{merge}: calculated according to Equation 3.3.

Before data collection, several test images were collected and processed with the program iMosflm, to determine the space group and calculate a best data collection strategy for the current crystal [94]. Three anomalous datasets were collected on a SeMet Tca17 crystal to around 3 Å resolution, and a native dataset was collected on another SeMet Tca17 crystal to 2.6 Å resolution. Some time later, another native dataset was collected on a manually grown SeMet Tca17 crystal to 1.8 Å resolution. All datasets were indexed and scaled with the XDS suite [95]. Accordingly, the crystals belong to space group C2, contain one Tca17 molecule in each asymmetric unit and therefore have a solvent content of 52% (calculated by the CCP4 program Matthews [111]). Data collection statistics are listed in Table 4.3.3.

4.3.6 Structure determination

The three anomalous diffraction datasets were uploaded and processed with the Auto-Rickshaw server at EMBL-Hamburg (see 3.3.5.1). The automatically built initial model was modified and improved manually in COOT, according to the experimental electron density map. Then the improved initial model was used to phase the 2.6 Å native dataset by molecular replacement with the program Molrep [112]. The atomic model of Tca17 could be improved to include 107 out of the 152 amino acids, with R_{work}/R_{free} values of 33% / 38%.

When a new native dataset of 1.8 Å became available, it was again phased by the molecular replacement method. The Tca17 model was further modified and improved by several rounds of manual modification in COOT and model refinement with REFMAC5, until convergence when the *R*-values and stereochemical parameters were satisfactory. Altogether, 143 amino acids (AAs) of Tca17 could be fitted in the electron density. Among them, 141 are from the 152 AAs of Tca17, and two additional AAs at the C-terminus are derived from the expression vector. Five AAs have alternative conformations, an example of which is shown in Fig 4.1.4. In addition to the atomic model of the Tca17 protein alone, one cloride ion, one glycerol molecule and 133 oxygen atoms from water molecules could be fitted into the electron density map, yielding final R_{work}/R_{free} values of 18.32% / 21.96% and no outliers in Ramachandran diagram (see Table 4.3.4 and Fig 4.3.5).

Number of refined atoms		**Ramachandran diagram (%) [104]**	
Protein / ligand / water	1189 / 7 / 133	**Most favored**	96.8
R_{work} / R_{free} (%)	18.32 / 21.96	**Additionally allowed**	3.2
Temperature factors (Å^2)		**Generously allowed**	0
Protein	31.89	**Disallowed**	0
Ligand / water	65.66 / 28.80		
r.m.s. deviations from standard geometry			
Bond lengths (Å)	0.0110		
Bond angles (°)	0.454		

Table 4.3.4 Refinement statistics of the Tca17 structure

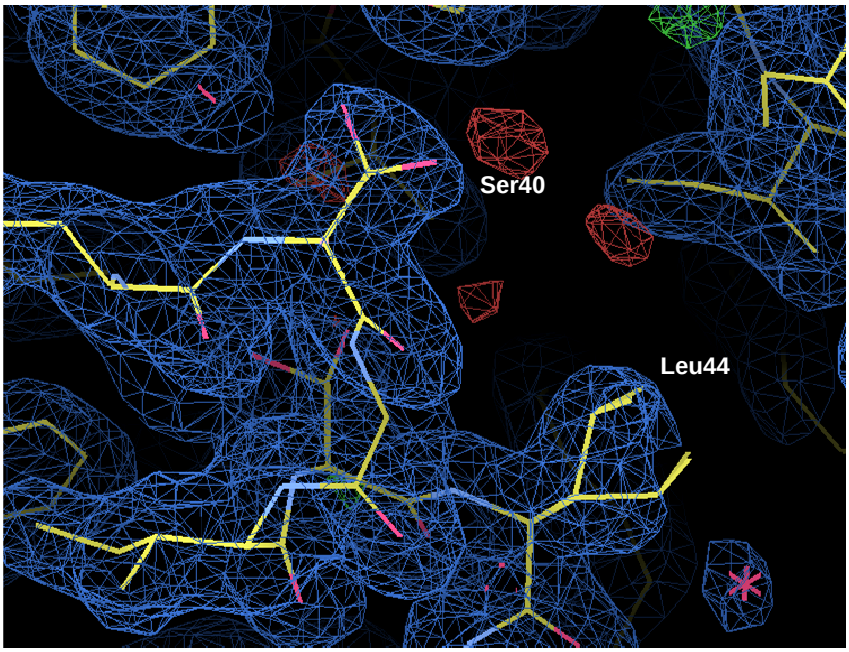

Fig 4.3.4 Alternative conformations of Ser40 and Leu44 in the structure of Tca17, figure prepared with COOT [102].
$2F_o$-F_c map contoured at 0.8 δ is shown in blue.
F_o-F_c map contoured at 3.0 δ and -3.0 δ is shown in green and red, respectively.

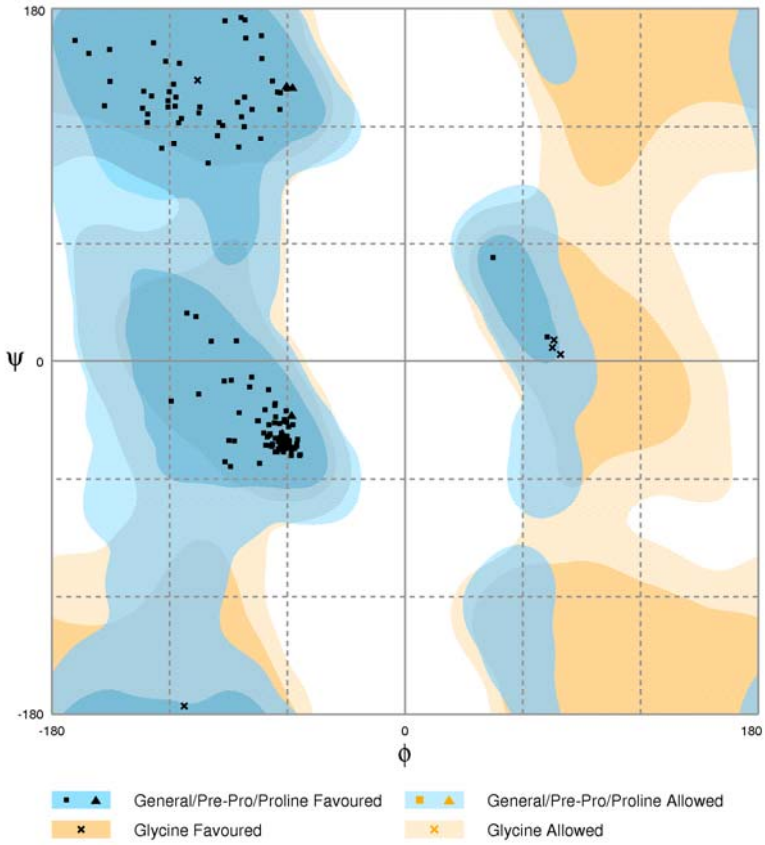

Fig 4.3.5 Ramachandran diagram of the Tca17 structure [113]

4.4 The structure of Tca17

4.4.1 Longin fold of Tca17 structure

In the crystal, one molecule of Tca17 is found in one asymmetric unit. The structure is arranged into a longin fold like other members of the Bet5 subfamily of TRAPP subunits (see Fig 1.3.4 c&d), in which a central β-sheet made up of five anti-parallel β-strands is flanked by one α-helix (α1) on one side and two α-helices (α2, α3) on the opposite side (see Fig. 4.4.1).

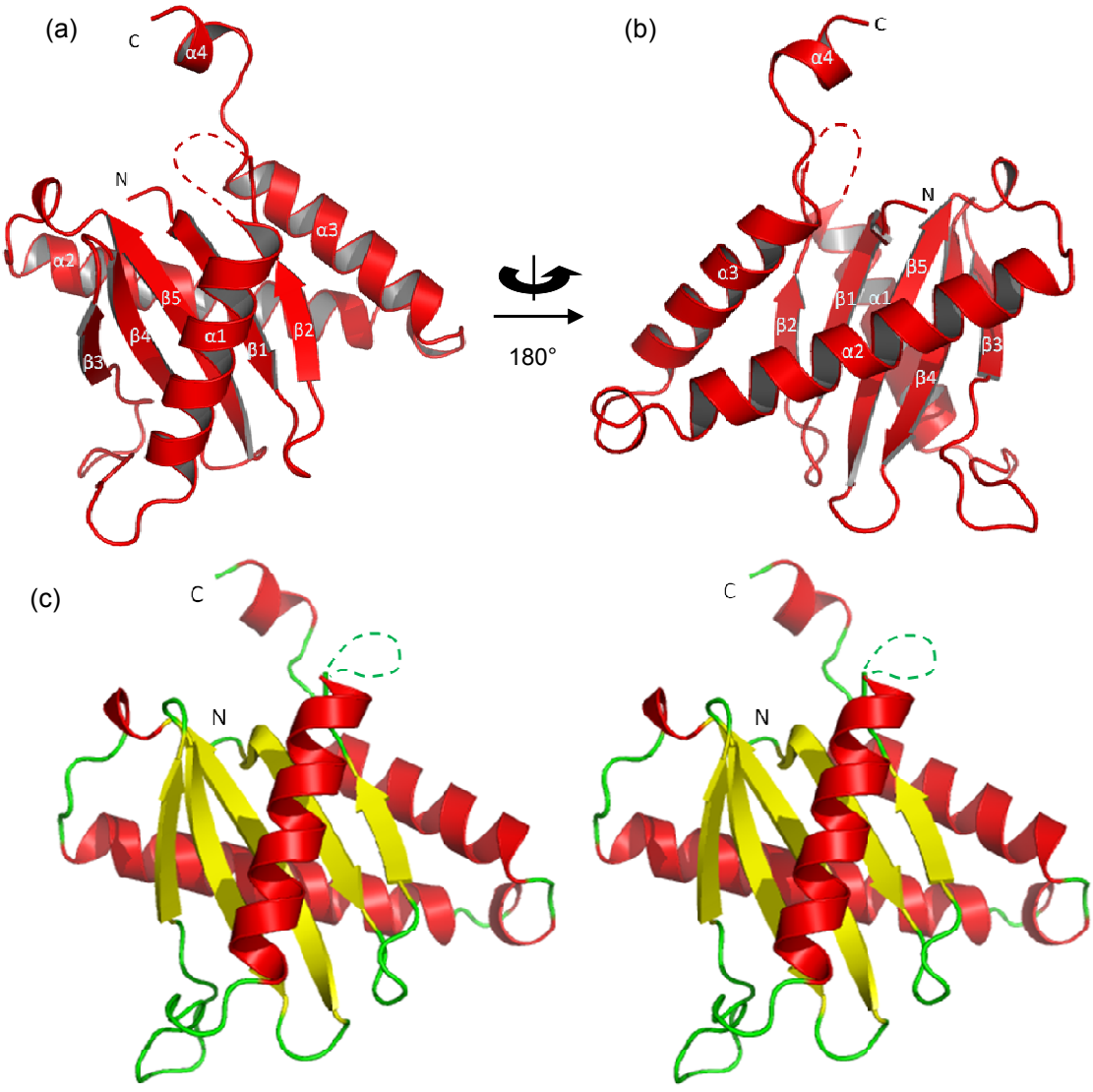

Fig 4.4.1 Cartoon representation of the Tca17 structure
(a) from one-helix side, (b) from two-helix side, (c) stereo view, colored according to secondary structure.
Unless stated otherwise, all protein structure figures in this chapter were prepared with Pymol [114]

The loop connecting β2 and α1 (AAs 25-31) as well as two residues at the N-terminus could not be traced in the electron density, probably due to local disorder. At the C-terminus of Tca17, two additional AAs coming from the expression vector were fitted to the electron density.

The secondary structure arrangement (5 β-strands and 4 α-helices) and surface accessibility of Tca17 structure is shown in Fig 4.4.2. The three central β-strands β1, β4 and β5 are more buried than the other two β-strands, while the loop regions and the last α-helix, α4 is well accessible for intermolecular contacts.

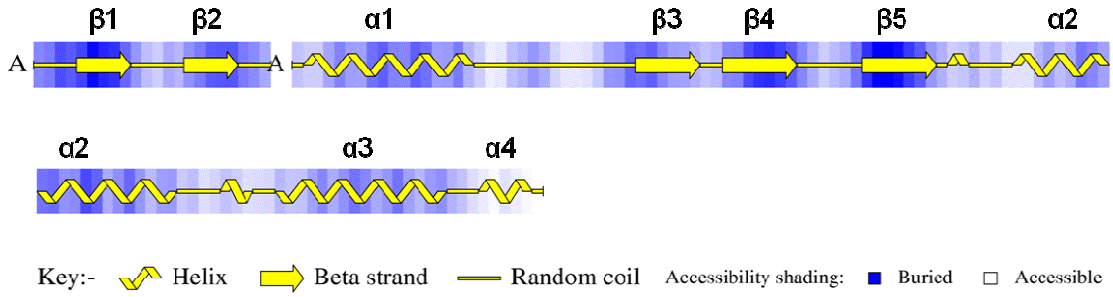

Fig 4.4.2 Secondary structure arrangement of Tca17 structure, shaded according to estimated accessibility, produced by PROCHECK [104]
A: Residues invisible in the structure.

The crystal packing of Tca17 structure is shown in Fig 4.4.3 a. The unit cell consists of four asymmetric units, as expected for a crystal belonging to space group C2. Each asymmetric unit contains one Tca17 molecule.

Unlike other members of the Bet5 subfamily (Fig 1.3.4 c&d), the C-terminus of Tca17 does not end right after α3, but extends further and forms an additional short helix α4. This short helix is extended away from rest of the Tca17 protein, but is stabilized by crystal contacts with symmetry-related molecule. A detailed view of the contacts in this interface is shown in Fig 4.4.3 b. Besides two hydrogen-bonds between residues T148, V150 and E70 of the symmetry-related molecule, this interface involves mostly hydrophobic interactions between several leucine and valine side chains.

The internal flexibility of Tca17 structure can be represented by the temperature factor, also called B-factor of each atoms in the structure. A cartoon representation of Tca17 structure, colored according to B-factor values of Cα atoms, is shown in Fig 4.4.4. From the result, the residues in last small helix α4 as well as some residues in α1, near the missing loop, are quite flexible. Whereas the residues away from this region are more stable. The B-factor difference between these two regions can be as high as 40 $Å^2$.

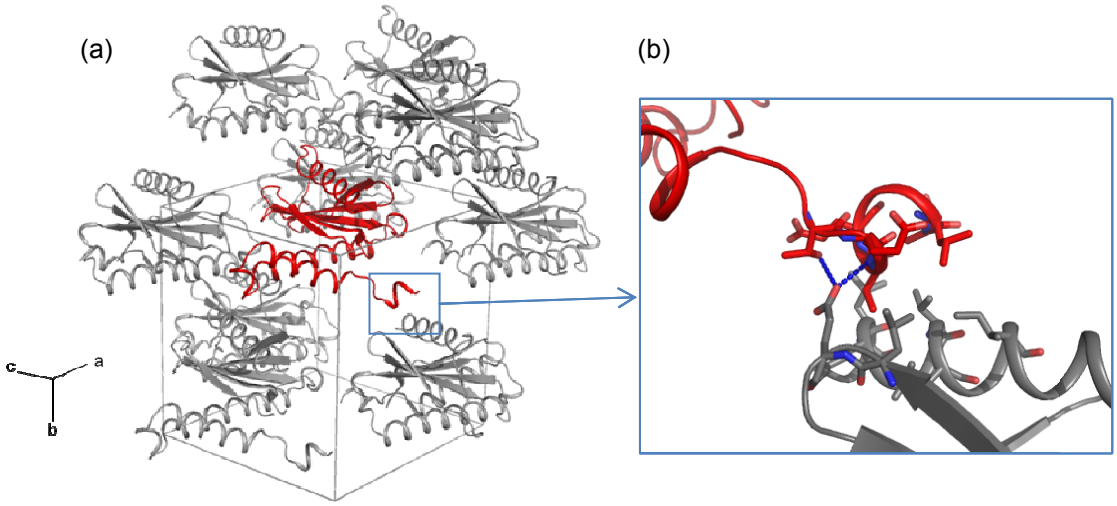

Fig 4.4.3 Crystal packing of Tca17
(a) Crystal packing of Tca17 with respect to the unit cell. One molecule of Tca17 is colored red, while the symmetry-related molecules are grey.
(b) Interaction between α4 of Tca17 and α1 of a symmetry-related molecule. All residues involved in interaction are shown as sticks. H-bonds at this interface are shown as blue lines.

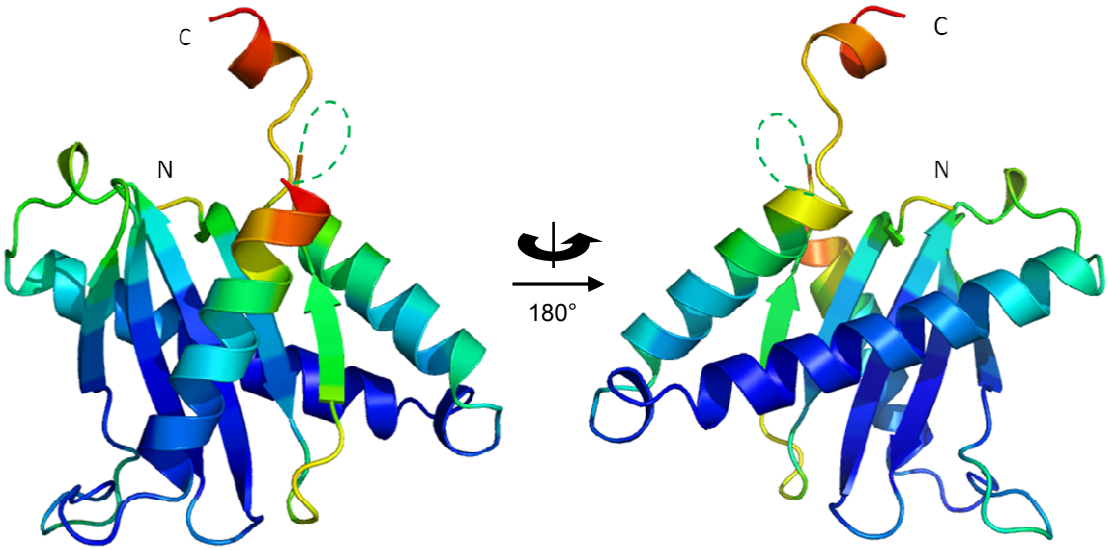

Fig 4.4.4 Cartoon representation of the Tca17 structure, colored by the B-factor values of Cα atoms. The regions with low B-factor values (< 20 Å^2) are shown in blue, while residues with high B-factor values (> 55 Å^2) are red.

4.4.2 Comparison with Bet5 subfamily proteins

In order to compare the structure of Tca17 with the structure of other Bet5 subfamily proteins in detail, a pairwise flexible structure alignment was performed with FATCAT (Flexible structure Alignment by Chaining Aligned fragment pairs allowing Twists) [115]. Unlike normal structure alignment programs, FATCAT does not treat proteins as rigid bodies, but divides them into aligned fragments. It simultaneously optimises the alignment and minimizes the number of rigid-body movements (twists) around hinges introduced in the reference protein. Therefore, the FATCAT approach is suitable for aligning distantly similar protein structures.

The structure of Tca17 was compared with yeast Bet5p (PDB id: 3CUE, chain C), mouse Bet5 (PDB id: 2J3T, chain C), yeast Trs23p (PDB id: 3CUE, chain A), human Trs23 (PDB id: 2J3T, chain D) and mouse sedlin (PDB id: 1H3Q). R.m.s. (root mean square) deviation values were calculated by FATCAT for aligned Cα atoms, with one structure rearranged, i.e. twists were introduced in the alignment. Sequence identity and similarity (amino acids with similar side chain properties occupying equivalent positions are considered similar) were also derived from the FATCAT structure alignment, which, considering the low similarity of all four proteins, is more reliable than alignments based on sequence alone (Table 4.4.1).

	Twist(s) introduced	**r.m.s.d (Å)**	**Equivalent Cα positions**	**Sequence identity (%)**	**Sequence similarity (%)**
Bet5p_yeast	0	3.00	111	11.8	23.0
Bet5_mouse	0	3.12	116	10.7	23.5
Trs23p_yeast	1	3.89	129	10.5	24.1
Trs23_human[a]	1	3.11	110	9.4	27.5
sedlin_mouse	1	2.88	124	12.6	28.5

Table 4.4.1 Structure comparison of Tca17 with other members of the Bet5 subfamily.
a: only the longin domain used in alignment.

The structure and sequence alignment allows the conclusion that, among the five proteins, mouse sedlin is the closest Tca17 relative. The structure and sequence similarity would be probably more obvious, if the structure of yeast Trs20p, the yeast sedlin ortholog, were available and could be used in a similar comparison.

4.4.3 Oligomerization state of Tca17

4.4.3.1 Disulfide-linked dimer-like arrangement in the crystal

In the crystal structure of Tca17, only one molecule was found in one asymmetric unit. However, a dimer-like arrangement of two Tca17 molecules related by a crystallographic screw axis was observed. In this arrangement, the two Cys121 side chains of either molecule are covalently linked by a disulfide bond (Fig 4.4.5). The only other cysteine residue, Cys6, is not involved in any disulfide bond.

(a)

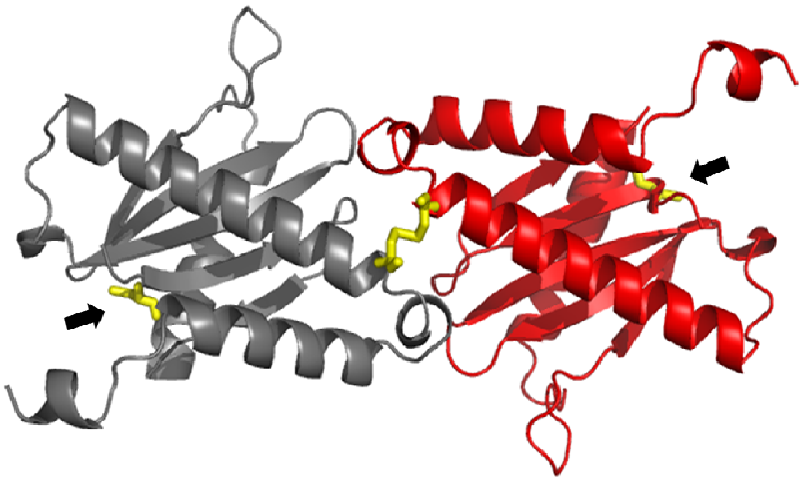

(b)

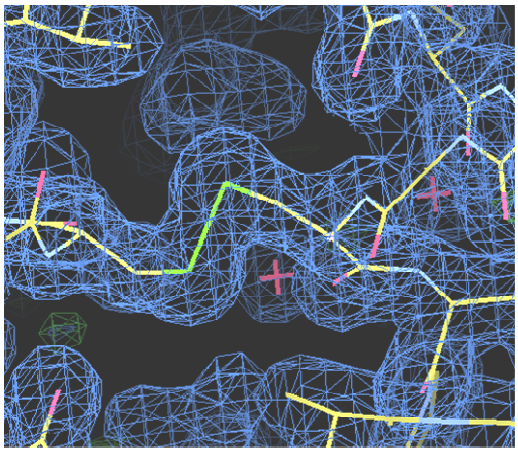

Fig 4.4.5 Disulfide-linked dimer of Tca17 in the crystal.
(a) Cartoon representation of the disulfide-linked dimer of Tca17 in the crystal. Cysteine residues are shown as yellow sticks. Disulfide bond formed by two Cys121 residues is shown in the middle, while the two Cys6 residues, free of any disulfide bond, are marked with arrows.
(b) Disulfide bridge between two Cys121 residues fitted into the electron density, prepared with COOT [102]. *2Fo-Fc* map contoured at 1.0δ is shown in blue.

The solvent-accessible surface area (SAS) per molecule buried in the dimer interface was calculated by the Pisa webserver [116] as 405 Å^2, corresponding to 4.7 % of the total SAS of a Tca17 monomer. This dimer interface is mainly stabilized by the single disulfide bond, which produces about 30 kcal/mole protein upon bond formation. If leaving out the disulfide bond, then the interface is only stabilized by hydrophobic interaction and surface contact, which produce about 3.5 kcal/mole protein upon dimerization. From these data one would expect that this dimer, in the absence of the disulfide bond, would be quite weak.

4.4.3.2 Monomer in solution

Analytical ultracentrifugation experiment:

In order to assess the oligomerization state of Tca17 in solution, a sedimentation velocity experiment of analytical ultracentrifugation (AUC) was performed, under similar buffer conditions as those used in protein crystallization. Two experiments were performed at Tca17 concentrations of 0.6 and 6.0 mg/ml, respectively, in SLS buffer (20 mM HEPES, pH 7, 300 mM NaCl, 5 mM βME, as listed in 2.4). From the sedimentation coefficient (*s*) distribution graph (Fig 4.4.6), only one main peak was present at either protein concentration, despite a minor trace of tailing toward higher *s* side, suggesting the protein sample was predominant present in one oligomerization form, while showing a small tendency toward higher oligomerization state.

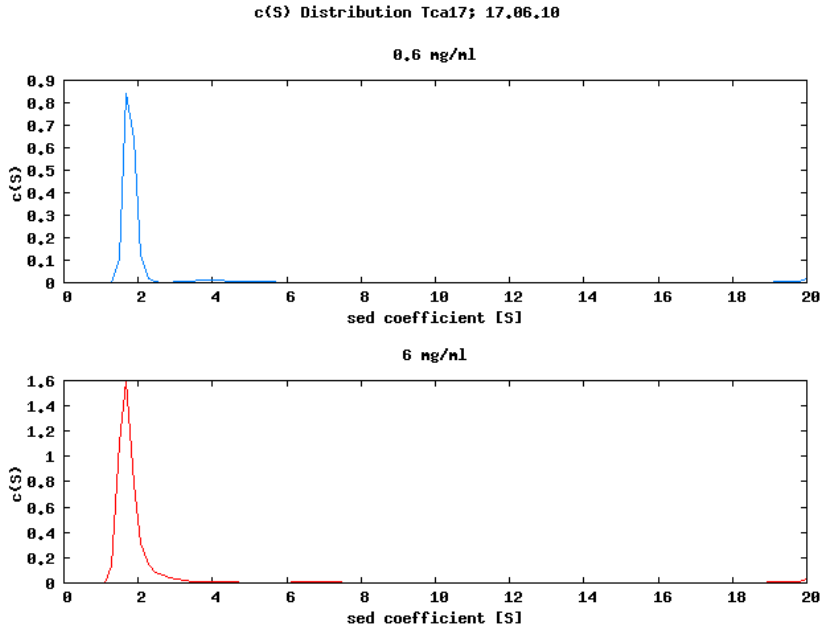

Fig 4.4.6 Sedimentation distribution of Tca17 in SLS buffer.

Values of the sedimentation coefficient (*s*) and the corresponding estimated molecular mass (*M*) are listed in Table 4.4.2. The estimated molecular mass values are closer to the calculated molecular mass of the Tca17 monomer (17.4 kDa) than the dimer (34.8 kDa). From the AUC data, it is therefore concluded that Tca17 is predominantly a monomer in SLS buffer.

Protein concentration (mg/ml)	***s***	***M* (kDa)***
0.6	1.779	18.1
6.0	1.768	21.4

Table 4.4.2 Estimated sedimentation and molecular mass of Tca17 in SLS buffer.
*: calculated by Equation 3.15.

Static light scattering:

For static light scattering (SLS) measurements, 100 µl of 7 mg/ml purified Tca17 were loaded onto a pre-equilibrated analytical gel filtration column (Superdex 75 10/300 GL), which was connected with a 2-angle SLS detector. The gel filtration elution profile and molecular weight curve of each elution peak estimated from SLS signal are shown in Fig 4.4.7.

For comparison, the SLS measurements were repeated with two different buffer conditions, the SLS buffer as used in analytical ultracentrifugation, and the SLS-2 buffer which had an equivalent NaCl concentration but no reducing agent. Before loading on the column, protein samples were dialysed against the appropriate buffers at 4 °C for 24 h, to ensure complete equilibration of the protein under the respective buffer conditions.

When the gel filtration was performed in SLS buffer, Tca17 eluted as one single peak representing one protein species with a molecular mass of ~16 kDa according to SLS (Fig 4.4.7 a), which is close to the molecular mass calculated from the sequence of Tca17. When the gel filtration was performed in SLS-2 buffer, this elution peak was slightly delayed, and the SLS analysis indicated a molecular mass of ~ 17 kDa. In addition, a faster migrating small peak was detected under SLS-2 buffer condition. The molecular mass of this protein species according to SLS analysis is ~35 kDa, consistent with a dimer of Tca17 (Fig 4.4.7 b).

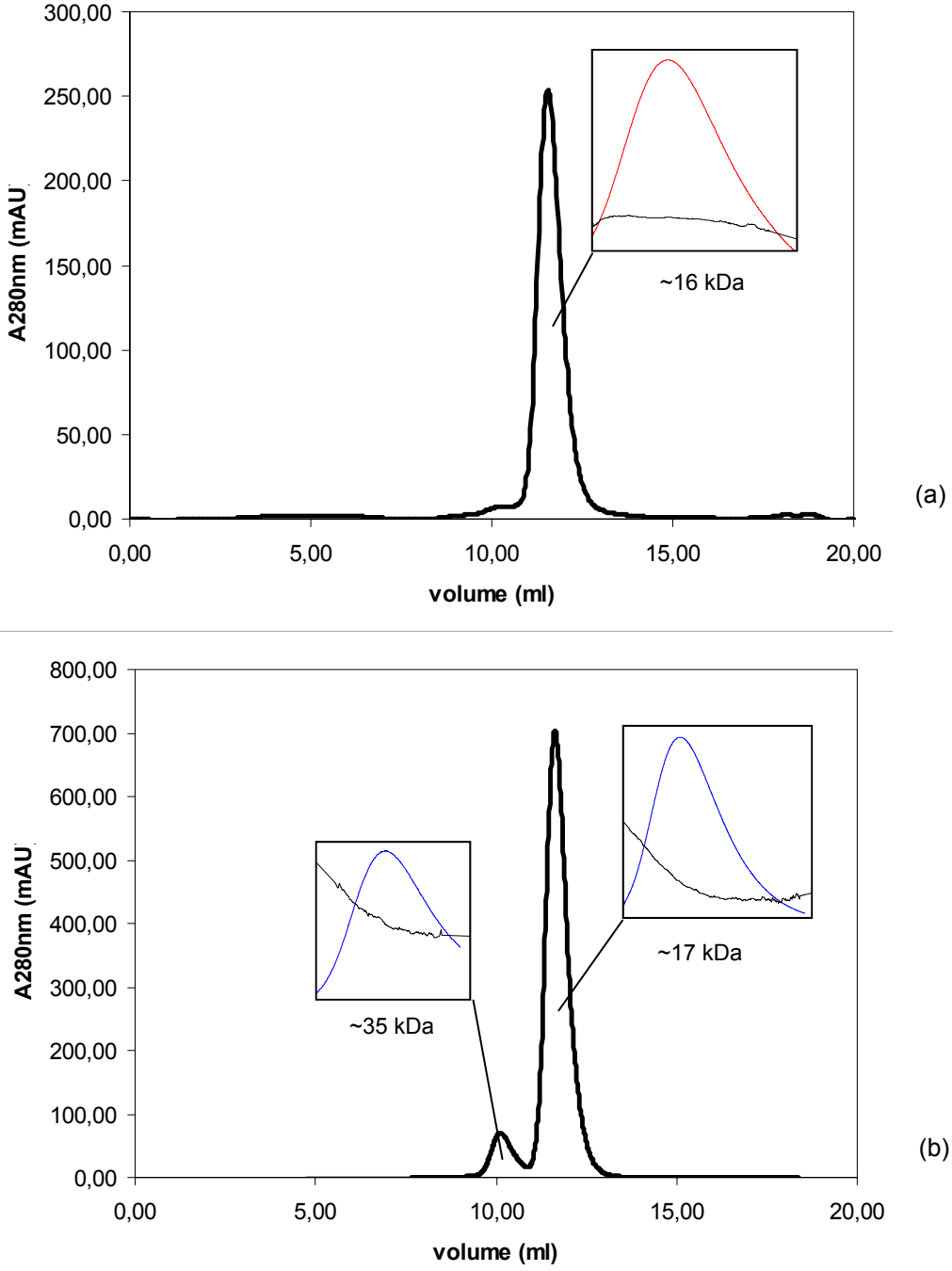

Fig 4.4.7 Gel filtration elution profiles and molecular masses detected by SLS, using (a) SLS buffer, and (b) SLS-2 buffer as running buffer.

The appearance of an apparently dimeric Tca17 species after gel filtration in non-reducing buffers indicates that the redox potential of the solution has an effect on the monomer-dimer equilibrium of Tca17. Although even in these buffers most of the protein (> 95%) remains monomeric, a non-reducing environment seems to favor dimer formation of Tca17. Disulfide bonds as observed in the Tca17 crystal structure require a non-reducing medium for their formation. It thus seems possible that the

minor species observed in non-reducing buffers indeed corresponds to disulfide-linked Tca17. There is no proof, however, that the dimeric Tca17 seen in this experiment is disulfide-linked.

Non-reducing SDS PAGE:

In order to prove whether the dimeric species of Tca17 is disulfide-linked, reducing and non-reducing SDS-PAGE were performed in parallel with purified Tca17 protein. The reducing protein samples were prepared by mixing Tca17 protein in Tca17 protein buffer with 2 x SDS sample buffer at 1:1 ratio, then boiling at 95 °C for 5 min. For the non-reducing protein samples, Tca17 solution was first dialysed against SLS-2 buffer for 24 h at 4 °C, then mixed with 2 x non-reducing SDS sample buffer at 1:1 ratio. (All buffers are listed in 2.4.) Both reducing and non-reduction protein samples were prepared at two different concentration, and loaded on one 15 % gel, with empty lanes in between to avoid unwanted reduction of the non-reducing samples. After Coomassie staining and proper destaining, the gel is shown as in Fig 4.4.8.

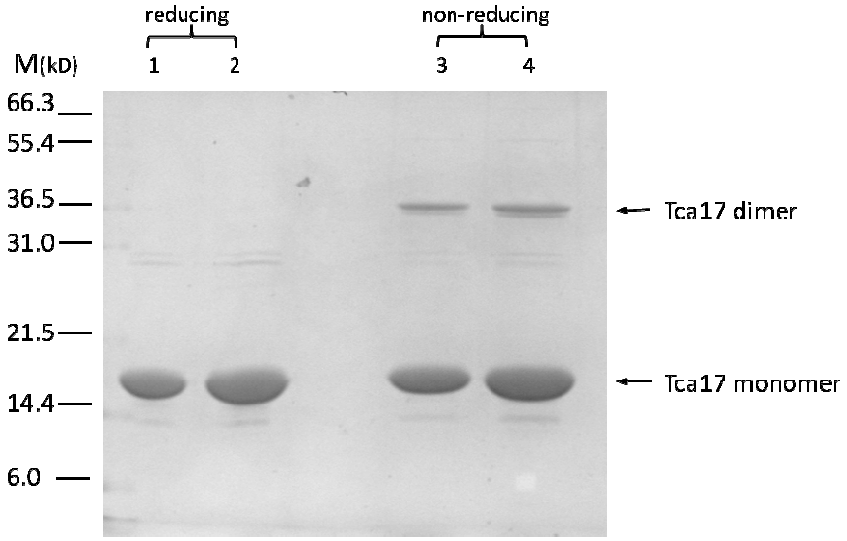

Fig 4.4.8 Reducing and non-reducing SDS-PAGE of purified Tca17 protein
1: 6 µg reducing sample, 2: 12 µg reducing sample,
3: 6 µg non-reducing sample, 4: 12 µg non-reducing sample.
The bands corresponding to Tca17 dimer (35 kDa) and monomer (17.5 kDa) were marked with arrows. By comparing with the marker lane, it was found that a small portion of Tca17 (< 5 %) appeared as dimer in the non-reducing protein samples.

From the gel, in the presence of reducing agent (50 mM DTT), Tca17 appeared as a clear monomer (MW = 17.5 kDa). Without the reducing agent, most of Tca17 (> 95%)

still remained as a monomer, whereas a small portion of dimeric species (MW = 35 kDa) was also detected. This dimer could not only be based on hydrogen bonds or hydrophobic interactions, since the presence of 1% SDS would break up these weak interactions. The result of non-reducing SDS-PAGE was in agreement with the SLS results, and further supported the conclusion that the dimeric Tca17 seen in SLS measurements and here in the gel was indeed disulfide-linked.

In the three experiments above, Tca17 is predominantly monomeric in reducing buffer conditions. In non-reducing buffer conditions, Tca17 remains mostly monomeric, while a small portion (< 5%) dimerizes.

In the crystallization processes, the protein solution starts from a reducing buffer condition (2 or 5 mM DTT is present in the protein buffer). During the long storage time (2-3 months at 4 °C), the reducing agent is gradually oxidized, leading to a disulfide bond formation, and hence further molecular contacts for crystal packing. However, from the *in vitro* experiments, it is also found that the dimeric species is only favored in a non-reducing environment. Therefore, in the reducing environment of yeast cell cytosol, a free Tca17 molecule should only be found as a monomer.

4.5 Interaction of Tca17 with TRAPP subunits

Although Tca17 was not formerly identified as TRAPP subunit, new evidence suggested that it interacted with Trs33p and Trs65p to help assemble or stabilize the TRAPP complex [82]. In this study, GST- and His- pull-down assays were performed to study the interaction between Tca17 and components of the TRAPP complex, hoping to under-stand the possible role of Tca17 in the regulation of TRAPP assembly and function.

In order to probe the interaction between Tca17 and yeast TRAPP subunits, considerable effort was invested to express and purify hepta-His tagged yeast TRAPP subunits from *E. coli*. Unlike their mammalian homologs, even the small yeast TRAPP subunits were quite insoluble or unstable when expressed in *E. coli*. Finally, only Bet3p and Trs33p could be produced in hepta-His tagged form and purified with good yield and quality.

A GST pull-down experiment using GST-Tca17 and tag-free Bet3p and Trs33p were performed according to the protocol in 3.4.3. After elution, pull-down results and controls were examined and compared with SDS-PAGE and coomassie staining. 1~2 μg of Bet3p and Trs33p proteins were also loaded on the gel as input controls.

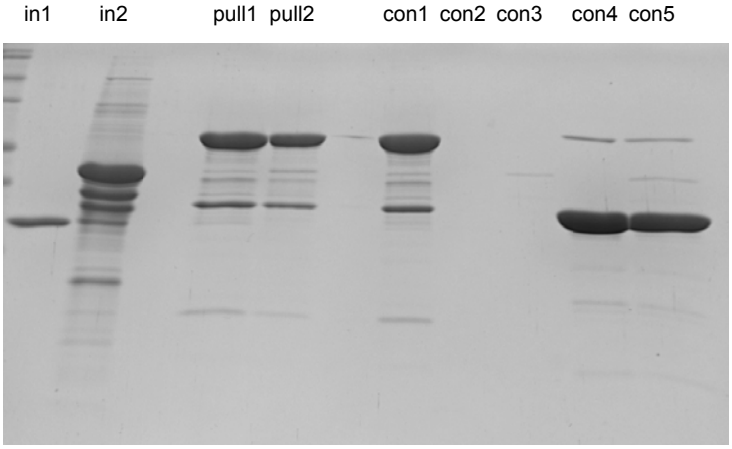

Fig 4.5.1 GST pull-down assays of Tca17 with yeast TRAPP subunits Bet3p and Trs33p In1, Bet3p input; in2, Trs33p input; pull1, Bet3p with GST-Tca17; pull2, Trs33p with GST-Tca17; con1, GST-Tca17 alone; con2, Bet3p alone; con3, Trs33p alone; con4, Bet3p with GST; con5, Trs33p with GST.

The GST pull-down result (Fig 4.5.1) failed to show clear binding of either Bet3p or Trs33p to GST-tagged Tca17.

A further trial to detect Tca17-Bet3p interaction was performed with His pull-down assay, using tag-free Tca17 and His_7-Bet3p, according to the protocol in 3.4.3. After elution, pull-down results and controls were examined and compared with SDS-PAGE and coomassie staining. Small about of tag-free Tca17 protein was also loaded on the gel as input control.

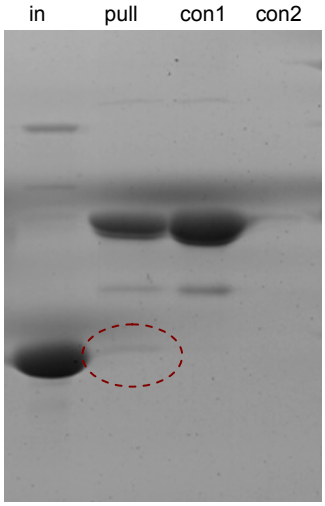

Fig 4.5.2 His pull-down assays of Tca17 with yeast TRAPP subunit Bet3p
In, Tca17 input; pull, Tca17 with His_7-Bet3p; con1, His_7-Bet3p alone; con2, Tca17 alone. A weak pull down signal of Tca17 is marked by a circle.

From the His pull-down result (Fig 4.5.2), a slight band corresponding to Tca17 co-eluted with His_7-Bet3p was visable. This suggested that a very weak binding was possible between Tca17 and Bet3p *in vivo*. In the cytoplasm of yeast cells, this interaction is probably quite weak and transient, or needs to be stablized via other factors. The proposal that Tca17 is only weakly or transiently bound to TRAPP is in agreement with the experiment by Yip *et al.* [76], who didn't detect Tca17 in the yeast TRAPP II complexed prepared by TAP-purification.